ACS OMEGA

http://pubs.acs.org/journal/acsodf

Article

Highly Efficient Gold Nano-Flower Optical Biosensor Doped in a Sol–Gel/PEG Matrix for the Determination of a Calcitonin Biomarker in Different Serum Samples

Walaa E. Omer, Maged A. El-Kemary, Mostafa M. Elsaady, Mona N. Abou-Omar, Ahmed O. Youssef, Ali A. Sayqal, Ayman A. Gouda, and Mohamed S. Attia*

Cite This: *ACS Omega* 2020, 5, 5629–5637

Read Online

ACCESS | Metrics & More | Article Recommendations | Supporting Information

ABSTRACT: We developed a novel, simple, sensitive, accurate, and precise method for the determination of calcitonin in different serum samples with medullar thyroid carcinoma. The designed flower-like thin film gold nanoparticles doped in a sol–gel/polyethylene glycol mold are used as an optical biosensor for the efficient determination of calcitonin. The sensor was characterized by transmission electron microscopy, scanning electron microscopy, X-ray diffraction, energy-dispersive X-ray microanalysis, and Fourier-transform infrared spectroscopy. The efficiency of the considered bio-sensor is done using the quencher calcitonin of the emission band at 360 nm of biomarker obtained at λ_{ex} = 333 nm in acetonitrile solvent. The sensing mechanism was based on fluorescence resonance energy transfer. The remarkable quenching of the fluorescence intensity at 360 nm of optical sensor by various concentrations of calcitonin was successfully used as an optical biosensor for the assessment of calcitonin for different serum samples of patients with medullar thyroid carcinoma. The calibration plot was prepared for the concentration range 0.01–1000 pg/mL of calcitonin with a correlation coefficient of 0.99 and a detection limit of 0.707 pg/mL. The suggested method augments the sensitivity of calcitonin as a useful biomarker for the early diagnosis of medullar thyroid carcinoma. This method is considered as a gateway for the construction of a new prototype for the follow-up of thyroid cancer in the spinal cord during and after treatment.

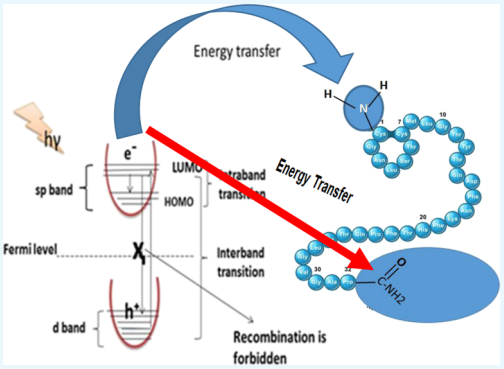

1. INTRODUCTION

The calcitonin (thyrocalcitonin) protein is a hormone present in humans and other mammals. This protein is secreted by parafollicular cells (C cells) of the thyroid gland. It consists of 32 amino acids, as shown in Figure S1.[1] Calcitonin withdraws calcium from the blood when the calcium concentration increases above the normal range. This occurs in different ways, such as (1) by reducing the activity of osteoclasts in bone tissues, thus preventing the desorption (breakdown) of bones. (2) By inhibiting the re-absorption of calcium by kidney cells, which in turn increases calcium secretion in urine.[2] An additional function of calcitonin is the reduction of the concentration of phosphorus in the blood when its level exceeds the normal value. Calcitonin is an excellent biomarker for medullar thyroid carcinoma (MTC).[3−6] The normal range of calcitonin is less than 18.2 pg/mL in males and 11.5 pg/mL in females.[7] Many methods are used to assess human serum calcitonin, such as radioimmunoassay,[8] time-resolved fluoroimmunoassay,[9] enzyme-linked immunosorbent assay (ELISA),[10] two-site immunofluorometry,[11] high performance liquid chromatography,[12] room-temperature phosphorescence immunoassay,[13] immunocytochemistry for calcitonin (ICC-calcitonin),[14] and electrochemical technique.[15] However, these methods have some disadvantages, such as the radioactive material contamination in radioimmunoassay is harmful to human health cell. Other immunoassay techniques necessitate a long time for analysis. Gold nanoparticles (Au NPs) are a good biosensor for the early diagnosis of diseases because of their distinct physical and chemical properties.[16] Accordingly, Au NPs can be used as a sensor according to different measured phenomena, such as electrochemical response,[17] photofluorescence,[18−21] UV–vis absorption,[22] and Raman scattering.[23] The interactions between Au NPs and some biomolecules are always very effective and specific.[24,25] Therefore, a highly selective and sensitive assessment method was obtained. Recently, we used them as a novel tool for the detection of pathogens[26] and unamplified *Aeromonas hydrophila* DNA.[27] We have witnessed the use of many sensitive

Received: September 2, 2019
Accepted: February 19, 2020
Published: March 12, 2020

https://dx.doi.org/10.1021/acsomega.9b02833
ACS Omega 2020, 5, 5629–5637

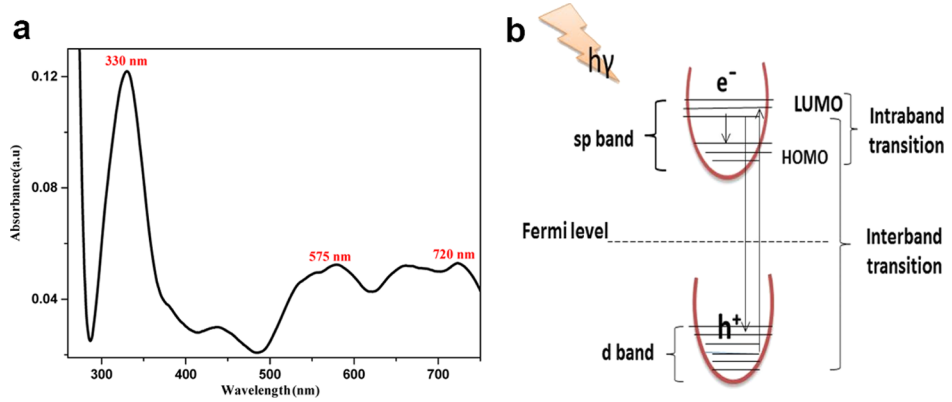

Figure 1. (a) UV−vis absorption spectrum of AuNFs in acetonitrile at 296 K. (b) Electronic transition in Au.

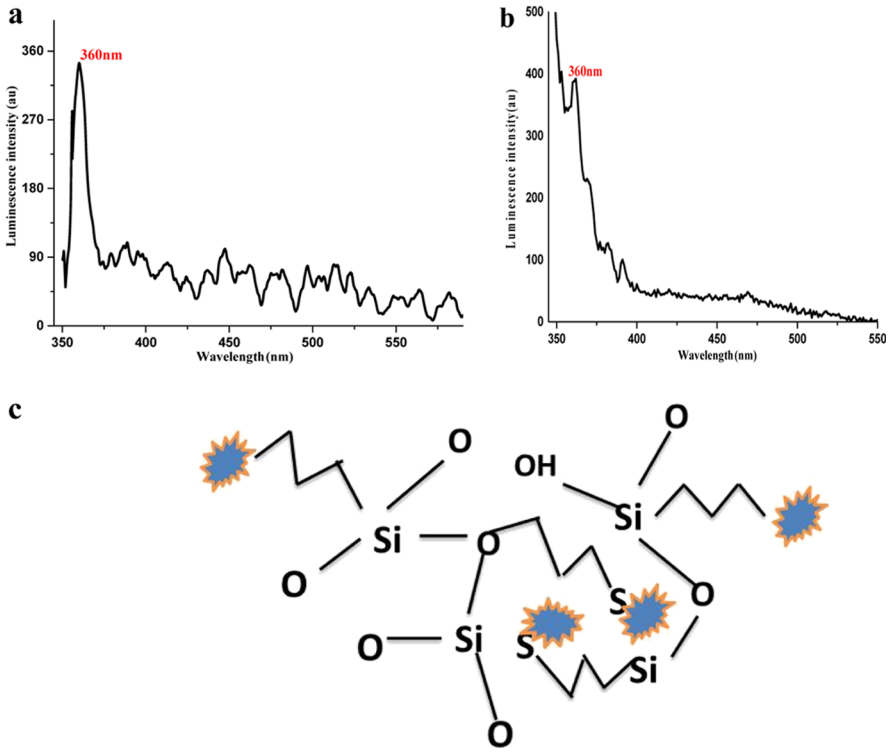

Figure 2. (a) Emission spectrum of the AuNF colloidal solution at λ_{ex} = 333 nm, (b) emission spectrum of AuNFs doped in the sol−gel matrix at λ_{ex} = 333 nm, and (c) AuNFs embedded in sol−gel.

NPs for cancer therapy.[28] In this work, the optical biosensor gold nanoflowers [AuNFs] doped in a sol−gel/polyethylene glycol (PEG) matrix draws our attention toward the sensitive determination of calcitonin medullar thyroid cancer biomarker in human serum because of its high sensitivity, simplicity, low cost, being relatively free from interference with coexisting substances, and relatively short analysis time than other methods. Using multi-branched NPs as an optical biosensor like AuNFs has more advantages in contrast to spherical NPs, such as strong plasmon resonances from the visible to near-infrared (NIR) regions which open the window to various biological applications. The roughened surface of the AuNFs increases the total surface area of the particle; therefore, the number of molecules that are able to attach to its surface have been increased. This property is used in surface-sensitive applications such as catalysis and surface-enhanced Raman scattering (SERS) because of its possible high-index facets. We have developed a three-dimensional (3D) AuNF film with high yield and good size monodispersity in the presence of a HEPES agent. The 3D AuNF film was used to detect calcitonin by measuring the fluorescence intensity of the nano-biosensor with various calcitonin concentrations in acetonitrile.

2. RESULTS AND DISCUSSION

2.1. Absorption Spectra. Figure 1a shows the UV−vis absorption spectrum of a AuNF colloidal solution in acetonitrile at 296 K. The observed spectrum has three absorption peaks in the ultraviolet, visible, and NIR regions. The first characteristic peak at 330 nm in the UV region represents the 5d−6sp transition, which is called the interband transition[29] that results from the absorption of higher energy photons. This phenomenon took place in gold because the outermost orbitals d and s might have hybridized together to

https://dx.doi.org/10.1021/acsomega.9b02833
ACS Omega 2020, 5, 5629−5637

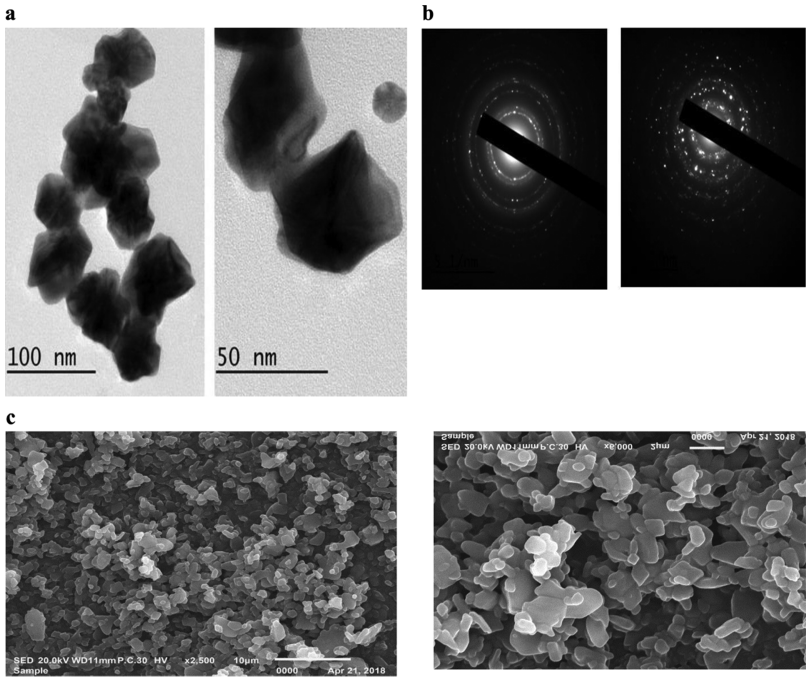

Figure 3. (a) TEM image of AuNFs, (b) SAED pattern of AuNFs, and (c) SEM image of AuNFs.

form six energy levels, five of which are flat and lie below the Fermi level, which are called d bands, and the sixth one lie above the Fermi level, which is called the conduction band or SP band (Figure 1b).[30] The second peak at 575 nm in the visible region might be due to the surface plasmon resonance effect,[31] which is caused by the collective oscillation of free electrons in the conduction band that resonated with the electromagnetic field of the incident light giving rise to intraband transition within the conduction band. The presence of two absorption bands in the visible and NIR regions is a characteristic feature of anisotropic AuNFs, which resulted from the free electrons in the conduction band oscillating on the short axis forming a transverse peak at 575 nm and on the long axis forming a longitudinal peak at 720 nm.[32−36]

2.2. Emission Spectra. Figure 2a shows the emission spectrum of the AuNF colloidal solution, in which an intensity peak is observed at 360 nm because of electron transition from the SP band to holes in the d band, leading to a recombination of high-energy electrons with high-energy holes producing high-energy photons. Other visible multiple emission peaks are due to different transitions from the lowest unoccupied molecular orbital (LUMO) levels to the highest occupied molecular orbital (HOMO levels) in the SP band. Figure 2b shows that the doped AuNFs in the sol−gel matrix have the same emission spectrum as the AuNF colloidal solution, which indicates that Au retains its morphology and size in the silica network, as shown in Figure 2c.

2.3. Characterization of AuNFs. Figure 3a shows the high-resolution transmission electron microscopy (TEM) images of AuNFs. The observed images of the synthesized particle are flower-like, which consist of a solid gold core with an average size of 48 ± 6 nm and irregular tips with an average size 10 nm. Figure 3b shows that selected area electron diffraction (SAED) is an important technique to determine the crystal structure of various materials. It is a complementary technique for TEM, in which the electrons are diffracted at a selected area, and bright spots with a dark background are observed as a result of that. From the SAED pattern, we obtain important information about the crystallinity of AuNFs with a polynanocrystalline shape (small spots making up rings, with each spot arising from the Bragg reflection of an individual crystallite). The scanning electron microscopy (SEM) images of AuNFs, as shown in Figure 3c, show the morphology and the roughness of the AuNF surface with a high surface area linking a large number of calcitonin molecules.

2.4. Characterization of the Thin Film Optical Biosensor. The Fourier-transform infrared (FTIR) spectra of the thin film of AuNFs doped in a sol−gel/PEG matrix are shown in Figure 4a. The spectrum of the thin film contains two bands centered at 1100 and 952 cm^{-1}, which are assigned to the $(Si-O-Si)_n$ and Si−OH stretching modes, respectively. This confirms the formation of polymeric silica as a result of hydrolysis and condensation of tetraethoxysilane (TEOS). Also, the presence of vibration modes at 526 cm^{-1} of M−O bonds (M = Au, Si) indicates the bonding between metallic ions and oxygen atoms in the xerogel network.[37] The vibration modes with energies at 2100 and 456 cm^{-1} are assigned to the Si−H stretching and Si−O−Si bending modes, respectively. As can be seen from Figure 4a, a comparison between the FTIR spectrum of thin film doped AuNFs with the spectrum of the film immersed in calcitonin solution shows that the intensities of some peaks are decreased. This is attributed to the adsorption of calcitonin onto the thin film surface.

The X-ray diffraction (XRD) pattern of the thin film of AuNFs doped in the sol−gel/PEG matrix is shown in Figure 4b. The XRD spectrum indicates the presence of gold in a face-centered cubic phase and revealed that AuNFs corresponded to the crystalline gold. The diffraction peaks at $2\theta = 38°$ (111), 44.13° (200), 64.35° (220), and 77.6° (311) are identical with those reported for the standard gold metal (Au^0).[38] The observed four intense peaks corresponding to the NPs are in agreement with the Bragg's reflections of gold identified with the diffraction pattern. Another diffraction peak at $2\theta = 25°$ (100) is assigned to SiO_2 of the matrix. The SEM image of the

https://dx.doi.org/10.1021/acsomega.9b02833
ACS Omega 2020, 5, 5629−5637

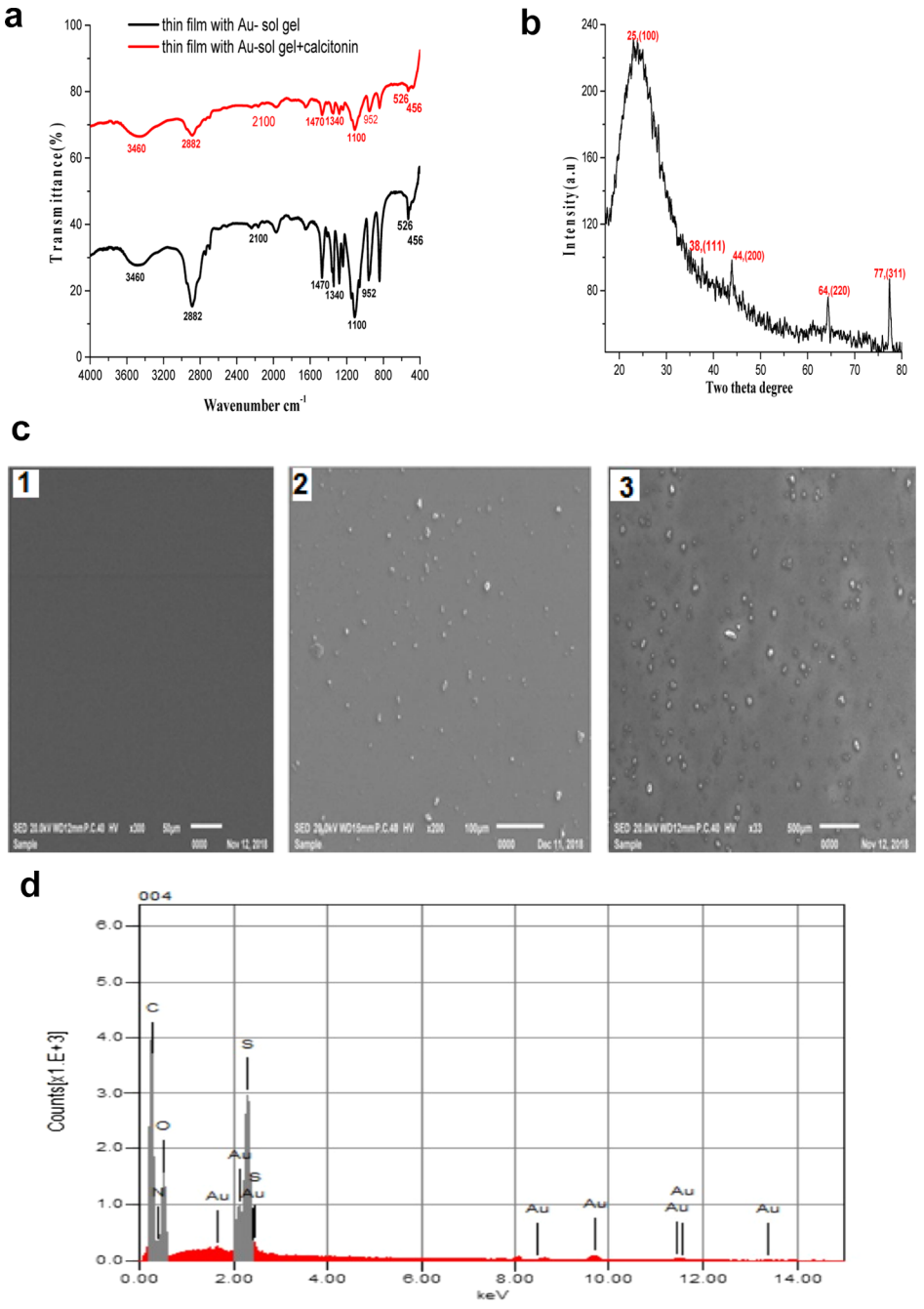

Figure 4. (a) FT-IR spectra of AuNFs doped in the sol−gel/PEG matrix thin film, (b) XRD pattern of AuNFs doped in the sol−gel/PEG matrix thin film, (c) (1) SEM image of the thin film with PEG only, (2) SEM image of the film of AuNFs/sol−gel/PEG matrix, (3) SEM image of the film of AuNFs/sol−gel/PEG matrix + calcitonin, and (d) EDX spectrum of AuNFs doped in the sol−gel/PEG matrix thin film.

thin film with the PEG matrix does not show any detectable particle on the film, as shown in Figure 4c1. However, a remarkable number of particles with a uniform distribution are observed on the SEM image of the thin film of AuNFs doped in the sol−gel/PEG matrix, as shown in Figure 4c2. In addition, for the thin film of AuNFs doped in sol−gel/PEG matrix + calcitonin, the SEM image shows that calcitonin molecules are physically adsorbed onto the surface of the gold sensor, as shown in Figure 4c3. The energy-dispersive X-ray (EDX) analysis using the SEM method was carried out to gain an insight about the elemental composition of the synthesized material. Figure 4d shows a typical EDX spectrum of AuNFs doped in the sol−gel/PEG matrix with C (46.5), O (45), Si (6.2), Au (2.3) wt % and C (55.05), O (39.72), Si (3.1), Au (2.13) wt %.

2.5. Analytical Parameters. Figure 5a shows the solvents' effect on the fluorescence intensity of the AuNF biosensor. The results revealed that the fluorescence intensity is significantly influenced by the solvent polarity, especially for acetonitrile, because acetonitrile has a moderate polarity between water and ethanol (protic solvents) and dimethylformamide and dimethyl sulfoxide (aprotic solvents). Therefore, acetonitrile protects the excited state of the AuNFs from any quenching sources. The effect of calcitonin concentration on the fluorescence intensity of AuNF biosensors was studied under the optimum conditions and is shown in Figure 5b. The

https://dx.doi.org/10.1021/acsomega.9b02833
ACS Omega 2020, 5, 5629−5637

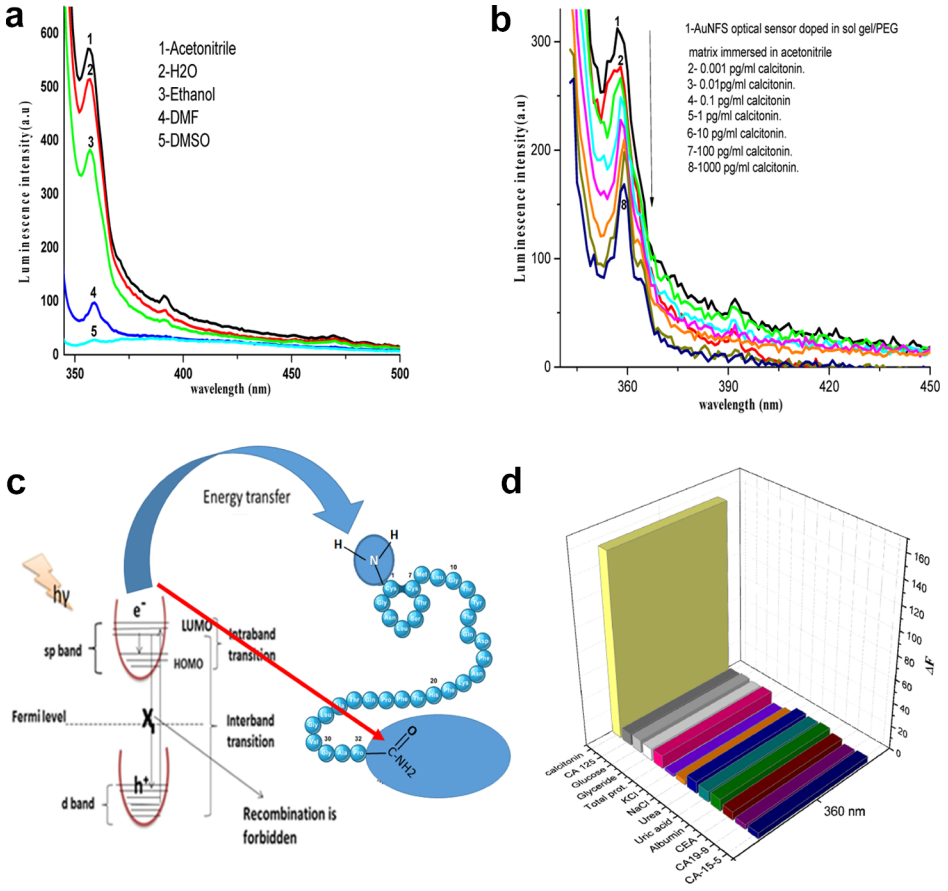

Figure 5. (a) Luminescence emission spectra of the optical sensor AuNFs-doped sol−gel/PEG thin film in different solvents at λ_{ex} = 333 nm, (b) fluorescence emission spectra of the thin film of AuNFs doped in the sol−gel/PEG matrix in different concentrations of calcitonin at λ_{ex} = 333 nm, (c) mechanism of quenching of the AuNF optical sensor by calcitonin, and (d) effect of the interfering ion concentration on the luminescence spectrum of AuNFs.

detection process was found to be the quenching of the fluorescence intensity of the AuNF biosensor by increasing the calcitonin concentration up to 1000 pg/mL. The mechanism of sensing depends on the energy transfer from the nano-optical AuNF biosensor in the excited state [surface plasmon resonance effect,[31] which is caused by the collective oscillation of free electrons in the conduction band that resonated with the electromagnetic field of the incident light giving the intraband transition within the conduction band] to the p-orbitals of NH_2 and $CONH_2$ terminal groups in the calcitonin protein, as shown in Figure 5c. This indicates a probable involvement of the dynamic quenching mechanism via energy transfer between the quencher and the optical sensor through electrostatic collision. This agrees well with the SEM and XRD results. The selectivity and the validity of the proposed method were examined by studying the effect of different interfering proteins, for example, CEA, CA 125, CA 19-9, CA 15-3, albumin (0.7 g L^{-1}), NaCl, KCl (2.0×10^{-3} mol L^{-1}), uric acid (0.08 g L^{-1}), total protein (0.01 g L^{-1}), urea (0.06 g L^{-1}), glucose (0.08 g L^{-1}), triglyceride (0.06 g L^{-1}), on the fluorescence spectrum of the AuNF biosensor thin film after the addition of [calcitonin]. The tolerable limit is the concentration of the added species individually causing a deviation lower than 3% of the fluorescence intensity under the optimum conditions of the biosensor. The results indicated no significant observed effect on the intensity, Figure 5d.

3. METHOD VALIDATION

3.1. Dynamic Range. The effect of calcitonin concentrations on the fluorescence intensity of the AuNF optical biosensor is shown in Figure 5b. From the Stern−Völmer plot, the critical concentration of the quencher and the effective distance between the quencher and the biosensor are $C_0 = 1/K_{sv}$ = 6.003 pg/mL and $R_0 = 7.35/C_0^{-1/3}$ = 13.3 Å, respectively. From the R_0 value [>10 Å] in the expected dynamic quenching mechanism, we can infer that an energy transfer has occurred between the quencher and the biosensor via electrostatic collision, which is consistent with the SEM and XRD results. Data are obtained from the Stern−Völmer plot of $[(F_0/F) - 1]$ versus [calcitonin], as shown in Figure S2. The fluorescence intensity at 360 nm decreases linearly with the concentration of calcitonin above the range 0.01−1000 pg/mL with a correlation coefficient of 0.99. The limit of detection (LOD) and the limit of quantification (LOQ) were calculated, as shown in Table S1, according to ICH guidelines.[39] Comparing the results obtained by the proposed AuNF biosensor with other reported methods,[14,40−46] the proposed method is found to have superior sensor stability, lower LOD (0.707 pg/mL), and applied wide linear range (0.01−1000 pg/mL).

3.2. Accuracy and Precision of the Method. The accuracy and precision of the suggested method were evaluated by carrying out the assessment three times in a day to determine the intraday precision and three times in different days to determine the average values for verifying the interday

https://dx.doi.org/10.1021/acsomega.9b02833
ACS Omega 2020, 5, 5629−5637

Table 1. Intraday and Interday Accuracy and Precision Calculation of the Proposed Method[a]

		intraday accuracy and precision (n = 3)			interday accuracy and precision (n = 3)		
samples	standard method average pg/mL	average found pg/mL ± CL	% RE	% RSD	average found pg/mL ± CL	% RE	% RSD
patient (1)	0.53	0.51 ± 0.21	3.77	1.10	0.54 ± 0.21	−1.89	1.00
patient (2)	0.52	0.52 ± 0.21	0.00	1.00	0.53 ± 0.21	−1.92	1.10
patient (3)	1.2	1.23 ± 0.14	2.50	0.51	1.15 ± 0.14	4.17	0.52
patient (4)	0.99	1.00 ± 0.15	1.01	0.09	1.10 ± 0.15	−11.1	0.02
patient (5)	18	18.1 ± 0.03	0.56	0.01	18.1 ± 0.03	0.56	0.19
patient (6)	23	23.02 ± 0.03	0.09	0.15	23.1 ± 0.03	−0.43	0.15
patient (7)	12	12.2 ± 0.04	1.67	0.29	12.3 ± 0.04	−2.50	0.29
patient (8)	34	34.16 ± 0.03	0.47	0.10	34.5 ± 0.03	−0.74	0.10
Patient (9)	93	93.06 ± 0.02	0.06	0.03	93.1 ± 0.02	−0.11	0.03
Patient (10)	125	125.2 ± 0.01	0.16	0.02	125.4 ± 0.01	−0.32	0.02

[a][% RE: relative error percentage, % RSD: percentage relative standard deviation, and CL = $\pm tS/\sqrt{n}$: confidence limits. t is the tabulated value = 4.303, at the confidence level = 95%; n = number of measurements; and S = standard deviation].

accuracy and precision of the method. These measurements were performed on four control and six test samples of the serum of patients with MTC. The results of this study are summarized in Table 1. The percentage relative standard deviation (% RSD) values of the proposed method were ≤0.006−1.1% (intraday) and ≤0.104−1.1% (interday). These results approved the high precision of the proposed method. Accuracy was assessed as percentage relative error (% RE) between the measured mean concentrations and the taken concentrations of calcitonin. Bias was calculated for each concentration {bias % = [(concentration found − known concentration) × 100/known concentration], and these results are also presented in Table 1. % RE values of ≤−2.50−3.77 (intraday) and ≤−2.50−4.17 (interday) demonstrate the high accuracy of the proposed method.

3.3. Application. The calcitonin (thyrocalcitonin) protein is a hormone present in humans and other mammals. This protein is secreted by parafollicular cells (C cells) of the thyroid gland.[47] Calcitonin withdraws the calcium from the blood when the calcium concentration increases above the normal range.

The analytical utility and applicability of the proposed method were tested by the assessment of calcitonin concentration in various serum samples (four samples of healthy persons and six samples of patients with MTC in the age range of 25−70 years). The obtained average values by the proposed method (4.16 ± 0.1 pg/mL) and (34.16 ± 0.02 pg/mL) match well with those obtained by the standard method (4.86 ± 0.17 pg/mL) and (35.16 ± 0.24 pg/mL) for serum samples of persons in the healthy state and patients with MTC, respectively, as shown in Table 1.

4. CONCLUSIONS

In this work, we developed a new method for assessment of calcitonin, which opens an excellent opportunity for a high-quality biomarker for the early diagnosis of MTC. The calcitonin was determined by doping the AuNF biosensor in the sol−gel/PEG matrix. The method depends on measuring the fluorescence intensity quenching of the thin film of the AuNF biosensor matrix under the optimized conditions. The established method is more sensitive because of its lower LOD of 0.707 pg/mL compared to the standard approach.

5. EXPERIMENTAL SECTION

5.1. Apparatus. All the equipment used in the present study are available in the Lab. of Prof. Dr. M. S. Attia at Chemistry Department, Faculty of Science, Ain Shams University and Institute of Nanoscience & Nanotechnology, Kafrelsheikh University. The absorption spectra of the samples were measured in the range of 200−800 nm with a Shimadzu UV-2450 double-beam spectrophotometer. All luminescence measurements were recorded on a Shimadzu RF5301PC spectrofluorometer in the range (200−800 nm). The FTIR spectra were measured with a JASCO FTIR-6800 in the range 400−4000 cm^{-1} using KBr pellets. The separation of protein from samples was carried out by centrifuging the sample for 15 min at 3000 rpm. The high-resolution imaging for the morphological investigation of the samples was performed using a JEOL JEM-2100 transmission electron microscope, Tokyo, Japan, with a resolution of 200 kV. A scanning electron microscope (Sirion from FEI) equipped with an EDX detector (S-3400N II, Hitachi, Japan) was used for the morphological investigation. The crystallinity and the phase structure of the materials have been studied using an X-ray diffractometer (Shimadzu 6000-XRD) using Cu Kα radiation (λ = 1.54056 Å).

5.2. Materials and Reagents. The starting materials $HAuCl_4$ (extra pure, about 51% Au, SLR, Fisher) and HEPES (≥99.5%, Sigma-Aldrich) were used as received. TEOS and PEG (MW 20,000) were purchased from Sigma-Aldrich. Calcitonin tumor marker was purchased from Alfa-Aesar. NaCl, KCl, albumin, uric acid, urea, and glucose were purchased from Sigma-Aldrich. High-purity distilled water obtained using a Milli-Q Plus system (Millipore Corp., Bedford, MA, USA) was used throughout for all measurements. All the other solvents were of high purity and obtained from Aldrich Chemical Company (USA). A stock solution of 0.5 mg/mL calcitonin was prepared by dissolving 0.5 mg of calcitonin in 1 mL deionized distilled water. Working solutions (0.001−1000 pg/mL) of calcitonin were prepared by accurate dilution of the stock solution with acetonitrile. Stock and working solutions were stored at 0−4 °C. The luminescence intensity was measured at $\lambda_{ex}/\lambda_{em}$ = 333/360 nm. Stock and working solutions were stored at 0−4 °C. The presence of CEA (130 U mL^{-1}), CA 19-9 (130 U mL^{-1}), CA 15-3 (130 U mL^{-1}), and CA 125 (150 U mL^{-1}) in combination with calcitonin in the serum sample of patients with MTC is considered a major problem in the assessment of calcitonin in

https://dx.doi.org/10.1021/acsomega.9b02833
ACS Omega 2020, 5, 5629−5637

the serum sample. To solve this problem, the microplate containing the calcitonin antibody was mixed with the serum sample of patients affected by MTC followed by washing with phosphate buffer to obtain only the calcitonin. The ΔF (ΔF is the subtraction of the luminescence intensity of the optical sensor without and with interfering species) value was calculated to determine the effect of the interfering species on the competence of the optical biosensor toward calcitonin. Human samples were obtained from the New Al Kasr El Aini Teaching Hospital, Cairo University and Ain Shams Specialized Hospital, Ain Shams University, Cairo, Egypt, in accordance with the WHO (World Health Organization)-approved protocol for human specimen collection and for the use of these materials and related clinical information for research purposes. All patients consented and approved the use of their clinical samples in the research work.

5.3. General Procedures. *5.3.1. Preparation of the Nano-Optical Sensor, AuNFs Doped in Sol–Gel/PEG Matrix.* 3D branched AuNFs with a solid core and more than 10 tips on their surface were synthesized by the limited ligand protection (LLP) strategy using a simple, template-free, and one-pot synthesis method with high yield and good size monodispersity at room temperature. The size of the AuNFs could be adjusted by controlling the molar ratio of $HAuCl_4$ to HEPES. A common Good's buffer, HEPES, was used as a weak reducing agent and a particle stabilizing agent to keep the growth of the AuNFs in 3Ds. AuNFs were synthesized by the following method.[48] In a typical experiment, 0.25 mL of 20 mM $HAuCl_4$ was added to 10 mL of a 20 mM HEPES solution (pH 7.4) without shaking. The formation of AuNFs was observed when the initial light-yellow mixture changed to pink and then to a turbid blue colloidal solution at room temperature within approximately 30 min, which can be used after 1 h. AuNFs were synthesized through a three-step mechanism: reduction of Au(III) ions to primary Au nanocrystals (step 1), agglomeration of the primary Au nanocrystals into intermediate agglomerates (step 2), and anisotropic growth of the agglomerates into gold flowers (step 3), Figure S3.

The AuNFs doped in sol–gel using the method reported in our previous work was then prepared.[49−57] The mixture consisting of TEOS, C_2H_5OH, and H_2O in a molar ratio of 1:5:1 was stirred for 15 min to obtain a homogeneous solution, and then 5 mL of AuNF precursor was added to the mixture with stirring for 5 min. Then, a few drops of diluted HCl solution were added as a catalyst. The mixture was refluxed for 1 h at 100 °C to obtain a precursor-dispersed sol solution, which was cast into a glass cup and kept at 25 °C until it cooled and then heated at 150 °C for 45 min to obtain a solidified and transparent composite, as shown in Figure S4.

A solution of the thin film was prepared by dissolving 0.1 g of the solidified and transparent sol–gel composite in 3 mL ethanol and then adding 10 mL of PEG with stirring for 1.0 h until a homogenous solution was obtained. A thin film was fabricated by spin-coating on a small quartz slide (width 8.5 mm, height 25 mm) to outfit the cuvette of the spectrofluorometer. First, the substrate slide was cleaned with distilled water and surfactant, then ultrasonically for 30 min in distilled water and surfactant, followed by ultrasonic cleaning for 10 min in acetone, and finally it was boiled for 10 min in 2-propanol. Before spin-coating, the substrate was washed with 2-propanol and spun until the film was fully dry. Then, the sol–gel solution was dropped onto a cleaned substrate with a micropipette and was spun at 3000 rpm for 30 s.

5.3.2. Recommended Procedure. An appropriate volume (200 μL) of various standard concentrations of calcitonin should be diluted to 10 mL with acetonitrile. The dilute solution was mixed with a thin film of optical sensing AuNFs doped in the sol–gel/PEG matrix in the quartz cell of a spectrofluorometer. The luminescence spectra were recorded at the excitation wavelength λ_{ex} = 333 nm. The optical sensor was washed with acetonitrile after each measurement and the calibration curve was built by plotting the luminescence intensity at λ_{em} = 360 nm on the y axis versus the calcitonin concentration on the x axis.

5.4. Assay Principle. *5.4.1. Standard Method for Calcitonin.* The calcitonin immunoassay is a two-site enzyme-linked immunosorbent assay for the measurement of the biologically intact 32 amino acid chain of calcitonin.[58−60] It uses two different mouse monoclonal antibodies to human calcitonin specific for well-defined regions on the calcitonin molecule. One antibody binds only to calcitonin 11−23, and this antibody is biotinylated, while the other antibody binds only to calcitonin 21−32, and this antibody is labeled with horseradish peroxidase [HRP] for detection. This method based on patient and control samples should be read using the 450 nm wavelength for calcitonin concentrations up to 300 pg/mL and using the 405 nm reading with calcitonin concentrations above 300 pg/mL. The results obtained from calibrator measurements are plotted as the curve of absorbance versus concentration, so the concentration of calcitonin in human serum samples is determined from this curve.

5.4.2. Assay Protocol. Calibrator, control, and sample (100 μL each) were put in appropriate wells, and then 50 μL of the working anti-CT−HRP conjugate was added to all the wells and incubated for 18 ± 1 h at 2−8 °C, and washed. The chromogenic solution (100 μL) was added to each well within 15 min following the washing step. The microliter plate was incubated for 30 min at room temperature avoiding direct sunlight, and then 100 μL of the stop solution was added to each well. The absorbance was read at 450 nm (reference filter, 630 or 650 nm) within 1 h, and the results were calculated.

5.4.3. Proposed Method for Calcitonin. A 0.2 mL portion of each human serum sample was mixed with 10 mL of acetonitrile and then centrifuged for 15 min at 3000 rpm to remove serum proteins, and then the supernatant was collected. The optical biosensor, AuNFs doped in the sol–gel/PEG matrix thin film, was immersed in 2 mL of each serum solution in the measuring cuvette, and the emission intensity was measured at 360 nm against the reagent blank before and after serum addition, and the optical biosensor thin film is washed with acetonitrile after each measurement. Therefore, the calcitonin concentration can be determined by comparing the measured intensity with the calibration plot. This method is used for further measurements of the MTC patient samples.

■ ASSOCIATED CONTENT

Supporting Information

The Supporting Information is available free of charge at https://pubs.acs.org/doi/10.1021/acsomega.9b02833.

Structure of calcitonin, Stern–Völmer plot between the calcitonin concentrations and fluorescence intensity of the optical sensor, mechanism of AuNF formation in HEPES, mechanism of synthesis of Au doped in sol–gel,

https://dx.doi.org/10.1021/acsomega.9b02833
ACS Omega 2020, 5, 5629−5637

and a table listing the sensitivity and regression parameters for the proposed method (PDF)

AUTHOR INFORMATION

Corresponding Author

Mohamed S. Attia − *Department of Chemistry, Faculty of Science, Ain Shams University, 11566 Cairo, Egypt;* orcid.org/0000-0001-6074-7366; Phone: +(202) 1229867311; Email: Mohamed_sam@yahoo.com, mohd_mostafa@sci.asu.edu.eg

Authors

Walaa E. Omer − *Institute of Nanoscience and Nanotechnology, Kafrelsheikh University, 33516 Kafr El-Shaikh, Egypt*

Maged A. El-Kemary − *Institute of Nanoscience and Nanotechnology, Kafrelsheikh University, 33516 Kafr El-Shaikh, Egypt*

Mostafa M. Elsaady − *Department of Chemistry, Faculty of Science, Ain Shams University, 11566 Cairo, Egypt*

Mona N. Abou-Omar − *Department of Chemistry, Faculty of Women for Arts, Science and Education, Ain Shams University, 11566 Cairo, Egypt*

Ahmed O. Youssef − *Department of Chemistry, Faculty of Science, Ain Shams University, 11566 Cairo, Egypt*

Ali A. Sayqal − *Chemistry Department, Faculty of Applied Sciences, Umm Al-Qura University, 24231 Makkah, Saudi Arabia*

Ayman A. Gouda − *Faculty of Public Health and Health Informatics, Umm Al-Qura University, 24231 Makkah, Saudi Arabia*

Complete contact information is available at: https://pubs.acs.org/10.1021/acsomega.9b02833

Notes

The authors declare no competing financial interest.

ACKNOWLEDGMENTS

The authors acknowledge the financial support provided by Dr. Mohamed S. Attia Lab, Department of Chemistry, Faculty of Science, Ain Shams University and Institute of Nanotechnology, Kafrelsheikh University.

REFERENCES

(1) Toledo, S. P. A.; Lourenço, D. M., Jr.; Santos, M. A.; Tavares, M. R.; Toledo, R. A.; de Menezes Correia-Deur, J. E. Hypercalcitoninemia is not pathognomonic of medullary thyroid carcinoma. *Clinics* **2009**, *64*, 699−706.

(2) D'Hondt, M.; Van Dorpe, M.; Mehuys, B.; Deforce, D.; De Spiegeleer, B. Quality analysis of salmon calcitonin in a polymeric bioadhesive pharmaceutical formulation: sample preparation optimization by DOE. *J. Pharm. Biomed. Anal.* **2010**, *53*, 939−945.

(3) Gagel, R. F.; Marx, S. J. Multiple endocrine neoplasia. In *Williams Text book of Endocrinology*; Larsen, P. R., Kronenberg, H. M., Melmed, S., Polonsky, K. S., Eds.; Saunders: Philadelphia, 2003; Vol. *10*, pp 1717−1762.

(4) Clark, J. R.; Fridman, T. R.; Odell, M. J.; Brierley, J.; Walfish, P. G.; Freeman, J. L. Prognostic Variables and Calcitonin in Medullary Thyroid Cancer. *Laryngoscope* **2005**, *115*, 1445−1450.

(5) Traugott, A.; Moley, J. F. Medullary Thyroid Cancer: Medical Management and Follow-Up. *Oncology* **2005**, *6*, 339−346.

(6) Trimboli, P.; Giovanella, L.; Crescenzi, A.; Romanelli, F.; Valabrega, S.; Spriano, G.; Cremonini, N.; Guglielmi, R.; Papini, E. Medullary thyroid cancer diagnosis: An appraisal. *Head Neck* **2014**, *36*, 1216−1223.

(7) Basuyau, J.-P.; Mallet, E.; Leroy, M.; Brunelle, P. Reference Intervals for Serum Calcitonin in Men, Women, and Children. *Clin. Chem.* **2004**, *50*, 1828−1830.

(8) Cavalier, E.; Carlisi, A.; Chapelle, J.-P.; Delanaye, P. Analytical quality of calcitonin determination and its effect on the adequacy of screening for medullary carcinoma of the thyroid. *Clin. Chem.* **2008**, *54*, 929−930.

(9) Rong, H.; Tørring, O.; Sääf, M.; Sjöstedt, U.; Sjöberg, H. E.; Bucht, E. Sensitive time-resolved fluoroimmunoassay of salmon calcitonin. *Clin. Chem.* **1994**, *40*, 1774−1777.

(10) Lynch, C.; Seth, R.; Bates, D. L.; Self, C. H. Calcitonin determination by a fast and highly sensitive enzyme amplified immunoassay. *J. Immunoassay* **1988**, *9*, 179−192.

(11) Rong, H.; Deftos, L. J.; Ji, H.; Bucht, E. Two-site immunofluorometric assay of intact salmon calcitonin with improved sensitivity. *Clin. Chem.* **1997**, *43*, 71−75.

(12) Buck, R. H.; Maxl, F. A validated HPLC assay for salmon calcitonin analysis. Comparison of HPLC biological assay. *J. Pharm. Biomed. Anal.* **1990**, *8*, 761−769.

(13) Liu, J.-M.; Huang, X.-M.; Zhang, L.-H.; Zheng, Z.-Y.; Lin, X.; Zhang, X.-Y.; Jiao, L.; Cui, M.-L.; Jiang, S.-L.; Lin, S.-Q. A specific Tween-80-Rhodamine S-MWNTs phosphorescent reagent for the detection of trace calcitonin. *Anal. Chim. Acta* **2012**, *744*, 60−67.

(14) Trimboli, P.; Guidobaldi, L.; Bongiovanni, M.; Crescenzi, A.; Alevizaki, M.; Giovanella, L. Use of fine-needle aspirate calcitonin to detect medullary thyroid carcinoma: A systematic review. *Diagn. Cytopathol.* **2016**, *44*, 45−51.

(15) Majdi, S.; Jabbari, A.; Heli, H.; Yadegari, H.; Moosavi-Movahedi, A. A.; Haghgoo, S. Electrochemical oxidation and determination of ceftriaxone on a glassy carbon and carbon-nanotube-modified glassy carbon electrodes. *J. Solid State Electrochem.* **2009**, *13*, 407−416.

(16) Jia, J.; Wang, B.; Wu, A.; Cheng, G.; Li, Z.; Dong, S. A Method to Construct a Third-Generation Horseradish Peroxidase Biosensor: Self-Assembling Gold Nanoparticles to Three-Dimensional Sol−Gel Network. *J. Anal. Chem.* **2002**, *74*, 2217−2223.

(17) Zhang, J.-J.; Gu, M.-M.; Zheng, T.-T.; Zhu, J.-J. Synthesis of gelatin-stabilized gold nanoparticles and assembly of carboxylic single-walled carbon nanotubes/Au composites for cytosensing and drug uptake. *Anal. Chem.* **2009**, *81*, 6641−6648.

(18) Zhang, S.; Huang, F.; Liu, B.; Ding, J.; Xu, X.; Kong, J. A sensitive impedance immunosensor based on functionalized gold nanoparticle-protein composite films for probing apolipoprotein A-I. *Talanta* **2007**, *71*, 874−881.

(19) Min, I.-H.; Choi, L.; Ahn, K.-S.; Kim, B. K.; Lee, B. Y.; Kim, K. S.; Choi, H. N.; Lee, W.-Y. Electrochemical determination of carbohydrate-binding proteins using carbohydrate-stabilized gold nanoparticles and silver enhancement. *Biosens. Bioelectron.* **2010**, *26*, 1326−1331.

(20) Oh, E.; Hong, M.-Y.; Lee, D.; Nam, S.-H.; Yoon, H. C.; Kim, H.-S. Inhibition assay of biomolecules based on fluorescence resonance energy transfer (FRET) between quantum dots and gold nanoparticles. *J. Am. Chem. Soc.* **2005**, *127*, 3270−3271.

(21) Wang, L.; Yan, R.; Huo, Z.; Wang, L.; Zeng, J.; Bao, J.; Wang, X.; Peng, Q.; Li, Y. Fluorescence resonant energy transfer biosensor based on upconversion-luminescent nanoparticles. *Angew. Chem., Int. Ed.* **2005**, *44*, 6054−6057.

(22) Pavlov, V.; Xiao, Y.; Shlyahovsky, B.; Willner, I. Aptamer-Functionalized Au Nanoparticles for the Amplified Optical Detection of Thrombin. *J. Am. Chem. Soc.* **2004**, *126*, 11768−11769.

(23) Li, J. F.; Huang, Y. F.; Ding, Y.; Yang, Z. L.; Li, S. B.; Zhou, X. S.; Fan, F. R.; Zhang, W.; Zhou, Z. Y.; Wu, D. Y.; Ren, B.; Wang, Z. L.; Tian, Z. Q. Shell-isolated nanoparticle-enhanced Raman spectroscopy. *Nature* **2010**, *464*, 392−395.

(24) Nam, J.-M.; Stoeva, S. I.; Mirkin, C. A. Bio-bar-code-based DNA detection with PCR-like sensitivity. *J. Am. Chem. Soc.* **2004**, *126*, 5932−5933.

(25) Marzouk, S. Y.; Seoudi, R.; Said, D. A.; Mabrouk, M. S. Linear and non-linear optics and FTIR characteristics of borosilicate glasses doped with gadolinium ions. *Opt. Mater.* **2013**, *35*, 2077−2084.
(26) El-Sheshtawy, A.; Moustafa, N. Y.; El-Kemary, M.; Salah, A.; Soliman, H. Gold Nanoparticles as a Novel Tool for Detection of Pathogens. *Risk in Contemporary Economy*; "Dunarea de Jos" University of Galati, Faculty of Economics and Business Administration, 2016; pp 465−473.
(27) Elsheshtawy, A.; Yehia, N.; Elkemary, M.; Soliman, H. Direct detection of unamplified Aeromonas hydrophila DNA in clinical fish samples using gold nanoparticle probe-based assay. *Aquaculture* **2019**, *500*, 451−457.
(28) Hanafy, N.; El-Kemary, M.; Leporatti, S. Micelles Structure Development as a Strategy to Improve Smart Cancer Therapy. *Cancers* **2018**, *10*, 238.
(29) Lance Kelly, K.; Coronado, E.; Zhao, L. L.; Schatz, G. C. The optical properties of metal nanoparticles: the influence of size, shape, and dielectric environment. *J. Phys. Chem. B* **2003**, *107*, 668.
(30) Attia, M. S.; Ramsis, M. N.; Khalil, L. H.; Hashem, S. G. Spectrofluorimetric assessment of chlorzoxazone and Ibuprofen in pharmaceutical formulations by using Eu-tetracycline HCl optical sensor doped in sol−gel matrix. *J. Fluoresc.* **2012**, *22*, 779−788.
(31) Nikoobakht, B.; El-Sayed, M. A. Preparation and growth mechanism of gold nanorods (NRs) using seed-mediated growth method. *Chem. Mater.* **2003**, *15*, 1957.
(32) Chang, S.-S.; Shih, C.-W.; Chen, C.-D.; Lai, W.-C.; Wang, C. R. C. The shape transition of gold nanorods. *Langmuir* **1999**, *15*, 701.
(33) Brioude, A.; Jiang, X. C.; Pileni, M. P. Optical properties of gold nanorods: DDA simulations supported by experiments. *J. Phys. Chem. B* **2005**, *109*, 13138.
(34) Yu; Chang, S.-S.; Lee, C.-L.; Chris Wang, C. R. Gold Nanorods: Electrochemical Synthesis and Optical Properties. *J. Phys. Chem. B* **1997**, *101*, 6661.
(35) Stern, O.; Völmer, M. über die Abklingzeit der Fluoreszenz. *Z. Phys.* **1919**, *20*, 183−188.
(36) Lakowicz, J. R.; Berndt, K. W. Lifetime-selective fluorescence imaging using an rf phase-sensitive camera. *Rev. Sci. Instrum.* **1991**, *62*, 1727.
(37) Rao, P. S.; Deshpande, S.; Blümmel, M.; Reddy, B. V. S.; Hash, T. Characterization of brown midrib mutants of sorghum (Sorghum bicolor (L.) Moench). *Eur. J. Plant Sci. Biotechnol.* **2012**, *6*, 71−75.
(38) Chen, R.; Wu, J.; Li, H.; Cheng, G.; Lu, Z.; Che, C.-M. Fabrication of gold nanoparticles with different morphologies in HEPES buffer. *Rare Met.* **2010**, *29*, 180−189.
(39) ICH Harmonised Tripartite Guideline. Validation of Analytical Procedures: Text and Methodology Q2(R1). *International Conference on Harmonisation of Technical Requirements for Registration of Pharmaceuticals for Human Use*: Geneva, 2005; pp 1−13.
(40) Cavalier, E.; Carlisi, A.; Chapelle, J.-P.; Delanaye, P. Analytical Quality of Calcitonin Determination and Its Effect on the Adequacy of Screening for Medullary Carcinoma of the Thyroid. *Clin. Chem.* **2008**, *54*, 929−930.
(41) Rong, H.; Tørring, O.; Sääf, M.; Sjöstedt, U.; Sjöberg, H. E.; Bucht, E. Sensitive time-resolved fluoroimmunoassay of salmon calcitonin. *Clin. Chem.* **1994**, *40*, 1774−1777.
(42) Lynch, C.; Seth, R.; Bates, D. L.; Self, C. H. Calcitonin Determination by a Fast and Highly Sensitive Enzyme Amplified Immunoassay. *J. Immunoassay* **1988**, *9*, 179−192.
(43) Rong, H.; Deftos, L. J.; Ji, H.; Bucht, E. Two-site immunofluorometric assay of intact salmon calcitonin with improved sensitivity. *Clin. Chem.* **1997**, *43*, 71−75.
(44) Buck, R. H.; Maxl, F. A validated HPLC assay for salmon calcitonin analysis. Comparison of HPLC biological assay. *J. Pharm. Biomed. Anal.* **1990**, *8*, 761−769.
(45) Liu, J.-M.; Huang, X.-M.; Zhang, L.-H.; Zheng, Z.-Y.; Lin, X.; Zhang, X.-Y.; Jiao, L.; Cui, M.-L.; Jiang, S.-L.; Lin, S.-Q. A specific Tween-80-Rhodamine S-MWNTs phosphorescent reagent for the detection of trace calcitonin. *Anal. Chim. Acta* **2012**, *744*, 60−67.
(46) Majdi, S.; Jabbari, A.; Heli, H.; Yadegari, H.; Moosavi-Movahedi, A. A.; Haghgoo, S. Electrochemical oxidation and determination of ceftriaxone on a glassy carbon and carbon-nanotube-modified glassy carbon electrodes. *J. Solid State Electrochem.* **2009**, *13*, 407−416.
(47) Toledo, S. P. A.; Lourenco, D. M.; Santos, M. A.; Tavares, M. R. Hypercalcitoninemia is not Pathognomonic of Medullary Thyroid Carcinoma. *Clinics* **2009**, *64*, 699−706.
(48) Xie, J.; Zhang, Q.; Lee, J. Y.; Wang, D. I. The synthesis of SERS-active gold nanoflower tags for in vivo applications. *ACS Nano* **2008**, *2*, 2473−2480.
(49) Attia, M. S. Spectrofluorimetric assessment of Ramipril using optical sensor Samarium ion-doxycycline complex doped in sol-gel matrix. *J. Pharm. Biomed. Anal.* **2010**, *51*, 7−11.
(50) Attia, M. S.; Othman, A. M.; Aboaly, M. M.; Abdel-Mottaleb, M. S. A. Novel Spectrofluorimetric Method for Measuring the Activity of the Enzyme α-l-Fucosidase Using the Nano Composite Optical Sensor Samarium(III)−Doxycycline Complex Doped in Sol−Gel Matrix. *Anal. Chem.* **2010**, *82*, 6230−6236.
(51) Attia, M. S.; Aboaly, M. M. Highly sensitive and selective spectrofluorimetric determination of metoclopramide hydrochloride in pharmaceutical tablets and serum samples using Eu^{3+} ion doped in sol−gel matrix. *Talanta* **2010**, *82*, 78−84.
(52) Attia, M. S.; Youssef, A. O.; Essawy, A. A.; Abdel-Mottaleb, M. S. A. A highly luminescent complexes of Eu(III) and Tb(III) with norfloxacin and gatifloxacin doped in sol-gel matrix: A comparable approach of using silica doped Tb(III) and Eu(III) as optical sensor. *J. Lumin.* **2012**, *132*, 2741−2746.
(53) Essawy, A. A.; Attia, M. S. Novel application of pyronin y fluorophore as high sensitive optical sensor of glucose in human serum. *Talanta* **2013**, *107*, 18−24.
(54) Elabd, A. A.; Attia, M. S. A new thin film optical sensor for assessment of UO22+ based on the fluorescence quenching of Trimetazidine doped in sol gel matrix. *J. Lumin.* **2015**, *165*, 179−184.
(55) Attia, M. S.; Al-Radadi, N. S. Nano optical sensor binuclear Pt-2-pyrazinecarboxylic acid −bipyridine for enhancement of the efficiency of 3-nitrotyrosine biomarker for early diagnosis of liver cirrhosis with minimal hepatic encephalopathy. *Biosens. Bioelectron.* **2016**, *86*, 406−412.
(56) Attia, M. S. Nano optical probe samarium tetracycline complex for early diagnosis of histidinemia in new born children. *Biosens. Bioelectron.* **2017**, *94*, 81−86.
(57) Attia, M. S.; Al-Radadi, N. S. Progress of pancreatitis disease biomarker alpha amylase enzyme by new nano optical sensor. *Biosens. Bioelectron.* **2016**, *86*, 413−419.
(58) Balamurugan, B.; Maruyama, T. Evidence of an enhanced interband absorption in Au nanoparticles: size-dependent electronic structure and optical properties. *Appl. Phys. Lett.* **2005**, *87*, 143105.
(59) Deftos, L. J. Immunoassay for human calcitonin. I. Method. *Metabolism* **1971**, *20*, 1122−1128.
(60) Chiririwa, H.; Muzenda, E. Synthesis, Characterization of Gold (III) Complexes and an in vitro Evaluation of their Cytotoxic Properties. *Proceedings of the World Congress on Engineering and Computer Science*; WCECS, 2014; Vol. *II*.

https://dx.doi.org/10.1021/acsomega.9b02833
ACS Omega 2020, 5, 5629−5637